


Entanglement Transition in a Monitored Free-Fermion Chain: From Extended Criticality to Area Law

O. Alberton, M. Buchhold[✉], and S. Diehl

Institut für Theoretische Physik, Universität zu Köln, D-50937 Cologne, Germany

 (Received 7 June 2020; revised 10 March 2021; accepted 29 March 2021; published 30 April 2021)

We analyze the quantum trajectory dynamics of free fermions subject to continuous monitoring. For weak monitoring, we identify a novel dynamical regime of subextensive entanglement growth, reminiscent of a critical phase with an emergent conformal invariance. For strong monitoring, however, the dynamics favors a transition into a quantum Zeno-like area-law regime. Close to the critical point, we observe logarithmic finite size corrections, indicating a Berezinskii-Kosterlitz-Thouless mechanism underlying the transition. This uncovers an unconventional entanglement transition in an elementary, physically realistic model for weak continuous measurements. In addition, we demonstrate that the measurement aspect in the dynamics is crucial for whether or not a phase transition takes place.

DOI: [10.1103/PhysRevLett.126.170602](https://doi.org/10.1103/PhysRevLett.126.170602)

Introduction.—Fingerprints of the competition between unitary and nonunitary dynamics are found in almost all aspects of modern quantum science. The spectrum ranges from radiative decay in driven two-level systems [1,2] to dephasing of trapped ions and cold atoms due to laser noise [3] or phonon-induced dissipation in electronic devices and color centers [4,5]. Nonunitary processes crucially affect quantum dynamics from single particles to the many-body realm.

One fascinating example is phase transitions in the entanglement entropy, which have been discovered in unitary circuit dynamics subject to local projective measurements [6–11]. Focusing on the entanglement properties of individual measurement trajectories $|\psi(\xi)\rangle$, where $\xi(t)$ is a realization of temporal randomness encountered in quantum mechanical measurements, a transition from an entangling evolution obeying a volume law to a disentangled evolution governed by an area law as a function of the measurement rate has been identified [12–19]. A characteristic trait of these transitions is that they manifest themselves in *state-dependent* observables $\hat{O}(\rho(\xi))$, with $\rho(\xi) = |\psi(\xi)\rangle\langle\psi(\xi)|$. For example, for the entanglement entropy of a subsystem A , $\hat{O}(\rho(\xi)) = -\log \rho_A(\xi)$, where $\rho_A(\xi)$ is the reduced density matrix on A —a highly nonlinear function of the state $\rho(\xi)$. Such entanglement transitions have been reported in several setups, including nonunitary circuit models and chains of interacting bosons subject to continuous measurements [20–26].

Here we focus on one of the most elementary models for the competition between unitary and nonunitary dynamics, free fermions on a periodic chain, subject to coherent hopping and local monitoring of the fermion particle number, which preserves the system’s $U(1)$ symmetry [27–30]. This model can be simulated efficiently on large

system sizes [27]. Moreover, it is natural in terms of physical implementations (although this does not guarantee straightforward observability of entanglement transitions): this scenario arises, e.g., for ultracold fermions in optical lattices, Rydberg atom arrays, or spin chains, where the local particle number (or magnetization) is measured via homodyne detection [29,30]. From a measurement theory point of view, the nonunitary monitoring evolution results from taking the temporal continuum limit of weak measurements of the local fermion particle number, implemented, for instance, by a weak, local coupling to a projectively measured photon bath [30–33].

We report two central findings. (i) We establish the existence of an extended, robust “weak-monitoring” regime, for which the entanglement entropy asymptotically grows logarithmically with the subsystem size. This previously unanticipated regime is reminiscent of a critical, conformally invariant phase of fermions in $(1+1)$ dimensions. We strengthen the analogy to conformal field theory (CFT) by examining the behavior of connected density-density correlations and the mutual information, both displaying clear signatures of conformal invariance.

(ii) For strong monitoring, the system undergoes a phase transition into an area-law phase obeying disentangling dynamics. At the critical point, which is located at a nonzero measurement strength, finite size scaling of the entanglement entropy provides strong indications for a Berezinskii-Kosterlitz-Thouless (BKT) scenario underlying the measurement-induced phase transition. We characterize both phases in terms of the entanglement entropy, the mutual information, and the connected density correlation function, and find evidence that the conformally invariant, weak measurement phase is left via the BKT mechanism.

Finally, we compare the measurement-induced dynamics with a nonunitary circuit evolution, which neglects the measurement backaction and violates probability conservation during the dynamics. While all considered protocols collapse onto the same Lindblad quantum master equation, the difference surfaces, however, once state-dependent observables are considered: Among the trajectory evolutions considered here, only physical measurement protocols exhibit an entanglement phase transition.

The entanglement phase diagram is displayed in Fig. 1. We confirm that the volume law realized at $\gamma = 0$ is unstable against infinitesimal monitoring $\gamma > 0$ [25,27]. It is instead replaced by an intriguing subextensive behavior, which has also been observed very recently for free fermions with complete spatiotemporal randomness [25], and in measurement-only protocols [34]. The opposite limit $\gamma^{-1} = 0$ lacks any entangling operations and is characterized by an area law. We find a phase transition from the logarithmic scaling behavior, with a γ -dependent effective central charge, to an area law at a finite γ_c (cf. Fig. 1), similarly to Ref. [34], accompanied by a sudden drop of the central charge to zero. The transition is, however, absent for

a nonunitary circuit protocol, where only the logarithmic regime is observed.

Trajectory evolution.—We consider free fermions on a half filled periodic chain of length L , which is described by the nearest-neighbor hopping Hamiltonian $H = \sum_l c_{l+1}^\dagger c_l + c_l^\dagger c_{l+1}$ with fermionic creation and annihilation operators c_l^\dagger, c_l . Furthermore, the local fermion densities n_l are continuously, weakly measured, i.e., monitored, by some external mechanism, yielding a non-unitary contribution to the Hamiltonian. Generically this includes a stochastic term $\sim i\xi_{l,t}n_l$ with random events $\{\xi_{l,t}\}$, such that the time evolution of a fermion pure state $|\psi(\{\xi_{l,t}\})\rangle$ follows a stochastic trajectory.

For the major part of our analysis, we consider the quantum state diffusion (QSD) protocol. Here, the monitoring of the fermion densities is implemented via their coupling to a set of continuous variable bath operators [36,37]. Paradigmatic examples include the positions of free particles (so-called pointers) [20,38] or the quadratures of a photon environment, which can be measured via homodyne detection to implement a QSD evolution with cold atoms [29,30]. The wave functions in the QSD protocol follow the evolution equation [31,36,37],

$$d|\psi\{\xi_{l,t}\}\rangle = \left[-iHdt + \sum_l \left(\xi_{l,t}\hat{M}_{l,t} - \frac{\gamma}{2}\hat{M}_{l,t}^2 dt \right) \right] |\psi\{\xi_{l,t}\}\rangle, \quad (1)$$

where $\hat{M}_{l,t} = n_l - \langle n_l \rangle_t$ [39]. The real-valued Gaussian noise $\xi_{l,t}$ has zero mean $\overline{\xi_{l,t}} = 0$ and covariance $\overline{\xi_{l,t}\xi_{m,t'}} = \gamma dt \delta_{l,m} \delta(t-t')$.

For reference, we compare our results to two additional trajectory evolution protocols. (i) The quantum jump (QJ) evolution, which realizes a monitoring dynamics with a discrete measurement noise [32,33,40] and displays qualitatively similar behavior as the QSD [41]. (ii) The continuous-time limit of a nonunitary circuit description (QSDc) [25,41], also known as “raw” quantum state diffusion [31,37,41], which does not correspond to any monitoring.

Numerical procedure.—The evolution equation (1) is quadratic in the fermion operators; thus any initial Gaussian state $|\psi_0\rangle$ remains Gaussian under time evolution. This enables efficient numerical simulation of Eq. (1), which is outlined in Refs. [27,41]. The full information of the Gaussian fermion density matrix and correlations is encoded in the correlation matrix $D_{l,j}(t,t') = \langle c_{l,t}^\dagger c_{j,t'} \rangle$. For a chain of length L , the von Neumann entanglement entropy $S_{\text{vN}}(l,L)$ for a subsystem A of length l can be obtained from the eigenvalues of the equal-time correlation matrix of subsystem A [43,44] (see also Ref. [41]).

In what follows we initialize the system in a short-range correlated Néel state $|\psi_0\rangle = |010101\dots01\rangle$ and evolve the different types of trajectories according to Eq. (1).

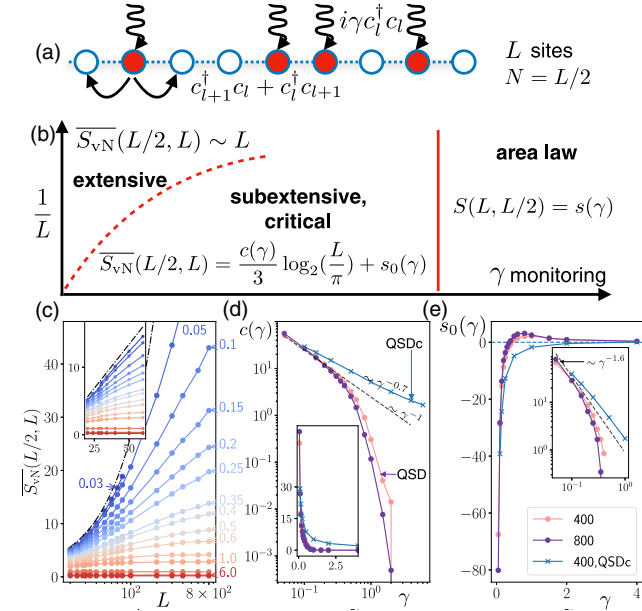


FIG. 1. (a) Free fermions hopping on a chain of length L subject to continuous monitoring with dimensionless rate γ . (b) Schematic “phase diagram” showing the different regimes of entanglement scaling with L (the dashed line denotes a finite size crossover). (c) At small monitoring rate, a subextensive growth of the entropy $\sim \log(L)$ at sufficiently large L is reminiscent of a critical, conformally invariant phase. For small γ, L , extensive growth $\sim L$ is observed (inset), approaching a volume law as $\gamma \rightarrow 0$. (d), (e) The effective central charge and residual entropy obtained by fitting the data to Eq. (2). The blue lines in (d) and (e) correspond to the nonunitary circuit evolution (QSDc), for which the transition is absent. The insets show the same data on a linear (d) and logarithmic (e) scale [35].

The entanglement entropy, mutual information, and correlation functions are computed for each individual trajectory after the evolution has reached a steady state, $\gamma t \gg 1$ [41]. We denote the trajectory average of an observable O by \bar{O} . The linear average $\bar{D} = \frac{1}{2}\mathbb{1}$ corresponds to an infinite temperature state for any $\gamma > 0$ and is independent of the trajectory evolution. For a nonlinear function of the correlation matrix $f(D)$, however, generally $\overline{f(D)} \neq f(\bar{D})$, and therefore $S_{\text{vN}}^-(l, L)$ cannot be obtained from the linear average \bar{D} .

Entanglement phase transition.—For a bipartition of the chain into two equal subsystems, the steady-state entanglement entropy $\overline{S_{\text{vN}}}(L/2, L)$ shows three different functional dependencies on the chain length L and the monitoring rate γ , as illustrated in Fig. 1(c) (see Ref. [41] for QJ). For the coherent time evolution at $\gamma = 0$, an initial Néel state develops an extensive entanglement entropy converging to a volume law [44]. This behavior transcends as a finite size effect to weak but nonzero monitoring, where an extensive entanglement growth $\overline{S_{\text{vN}}}(L/2, L) \sim L$ is observed for $L < L_c(\gamma) \sim \exp(\sqrt{\gamma_0/\gamma})$ smaller than a γ -dependent cutoff length [see, e.g., inset of Fig. 1(c)].

For any nonzero monitoring rate $0 < \gamma < \gamma_c$, and below a critical rate γ_c , the entanglement in the thermodynamic limit follows a subextensive growth $S \sim \log L$. This is characteristic for (1 + 1)-dimensional CFTs [45,46]. Here, we describe this growth according to a CFT with periodic boundaries,

$$\overline{S_{\text{vN}}}(l, L) = \frac{c(\gamma)}{3} \log_2 \left[\frac{L}{\pi} \sin \left(\frac{\pi l}{L} \right) \right] + s_0(\gamma), \quad (2)$$

but with a γ -dependent *effective* central charge $c(\gamma)$ and residual entropy $s_0(\gamma)$; see Figs. 1(d) and 1(e). Irrational or continuous central charges are established in CFTs for disordered or percolation problems [7,47–50] and have been recently reported for entanglement transitions as well [7,17,24,25,34]. An extended regime of logarithmic scaling of $\overline{S_{\text{vN}}}(l, L)$ was observed recently for a free, nonunitary circuit dynamics with spatiotemporal randomness [22]. Here, we establish an extended phase of measurement-induced conformal invariance for free fermions on a regular lattice.

A major finding of our work is the existence of a phase transition at a critical monitoring rate γ_c , above which conformal invariance is lost and the entanglement entropy obeys an area law. This transition is well illustrated in the behavior of the effective central charge $c(\gamma)$. For weak monitoring, $c(\gamma) \sim \gamma^{-1}$ decays algebraically and saturates at a nonzero value for $L \rightarrow \infty$. At stronger monitoring, the effective central charge, and therefore the logarithmic scaling, vanish above a critical value γ_c in the limit $L \rightarrow \infty$. For any finite size $L < \infty$, $c(\gamma)$ approaches zero according to an exponential $\log c(\gamma) \sim -|\gamma - \gamma_c(L)|^{-\alpha(L)}$

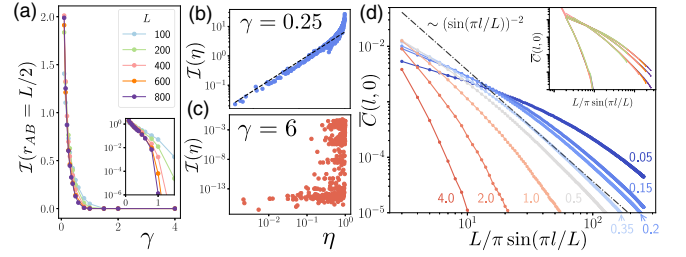


FIG. 2. The conformal invariance at weak monitoring is confirmed (a) by a large, nonzero mutual information $I_A = I_B = L/2$, which rapidly decays to zero in the area-law regime, and (b) by a scaling collapse of the mutual information as a function of the cross ratio η , i.e., $\mathcal{I}(\eta) \sim \eta$ ($L = 400$). (c) In the area-law regime no collapse is observed. (d) Equal-time correlations $\bar{C}(l, 0)$ decay algebraically $\sim l^{-2}$ (exponentially) with the distance l in the conformally invariant (area-law) regime ($L = 800$). The inset shows a data collapse for different system sizes $L = 200, 400, 600, 800$ (axes range as in main plot).

for some $\alpha(L) > 0$ [see Fig. 3(c)]. The phase transition is evidenced by a set of different, unambiguous observations: (i) a qualitative change in the entanglement entropy, which no longer shows any subsystem dependence for $\gamma \geq \gamma_c(L)$ [$\gamma_c(L = 800) \approx 0.8$ in Fig. 3(a)], (ii) the behavior of the effective central charge with γ in Fig. 1(d), as well as with the system size L in Fig. 3(c), which drops to zero for $\gamma > \gamma_c$ and $L \rightarrow \infty$, (iii) the zero crossing of the residual entropy $s_0(\gamma)$ in Fig. 1(e), which is required for a well-defined, positive entanglement entropy when $c \rightarrow 0$, and

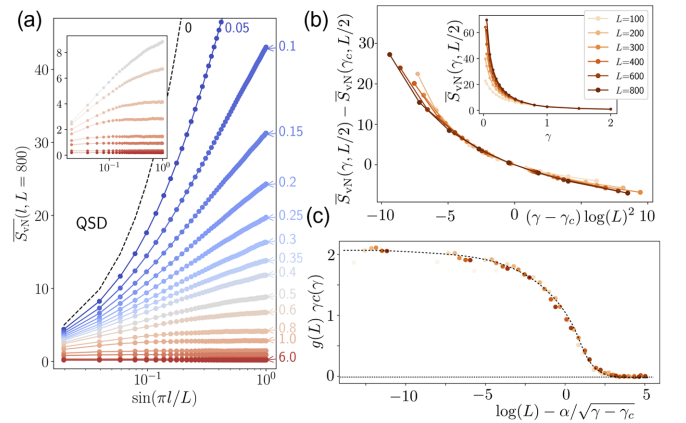


FIG. 3. (a) The entanglement entropy as a function of the bipartition size l reveals a clear, asymptotic logarithmic growth for weak monitoring and shows a transition to an area law for stronger monitoring $\gamma \geq \gamma_c$ (inset). (b) Finite size scaling collapse of the entanglement entropy, assuming BKT scaling of the correlation length and $\gamma_c = 0.31$ (the inset shows the unrescaled data). (c) Finite size scaling of the effective central charge, predicting a jump of $c(\gamma)$ from $c(\gamma_c - 0^+) \approx 2/\gamma_c$ to $c(\gamma_c + 0^+) = 0$ in the limit $L \rightarrow \infty$ (dotted lines are guides to the eye). The parameters are $\alpha = 3.99$, $\gamma_c = 0.21$, $g(L) = \{1 + 1/[2 \log(L) - 4.37]\}^{-1}$, and the legend from (b) applies in (c).

(iv) qualitative changes of the mutual information and the correlation function, shown in Fig. 2 and discussed next.

Mutual information.—The mutual information $\mathcal{I}(l_A, l_B)$ between two disjoint subsystems $A=[m_1, m_2]$, $B=[m_3, m_4]$ of length l_A, l_B has emerged as a useful indicator to locate an entanglement transition [17]. It is given by $\mathcal{I}(l_A, l_B) = S_{\text{vN}}(l_A, L) + S_{\text{vN}}(l_B, L) - S_{\text{vN}}(A \cup B, L)$, where $S_{\text{vN}}(A \cup B, L)$ is the entanglement entropy of the subsystem $A \cup B$. $\mathcal{I}(l_A, l_B)$ measures the amount of information that can be gained about subsystem A from subsystem B and vice versa, and it is also an upper bound for connected correlation functions between A and B [51]. For two disjoint intervals $l_A = l_B = L/8$, with centers at a distance $r_{AB} = L/2$, it is expected to show a sharp peak at the critical point separating the area- and the volume-law phase [17]. Inspecting $\mathcal{I}(l_A = l_B = L/8, r_{AB} = L/2)$ for different system sizes in Fig. 2(a) shows that it is significantly larger than zero in the entire critical regime and approaches zero rapidly in the area-law phase, reflecting extended criticality. A similar peak is observed for the QJ evolution [41].

For variable subsystem sizes, it is useful to define the cross ratio $\eta = m_{12}m_{34}/m_{13}m_{24}$ with $m_{\alpha\beta} = \sin(\pi|m_\alpha - m_\beta|/L)$. In the conformally invariant regime, the mutual information $\mathcal{I}(\eta)$ collapses onto a single line for all η , with a linear increase $\sim \eta$ for small cross ratios; see Fig. 2(b). The linear dependence in η also implies a power-law decay of the mutual information $\mathcal{I} \sim r_{AB}^{-2}$ for small subsystems with large separation [17]. This collapse is a strong signature of conformal invariance and can be observed throughout the entire logarithmic regime. It can be contrasted with the behavior in the area-law phase, shown in Fig. 2(c), where no collapse is observed.

Correlation function.—In addition, we detect signatures of conformal invariance in connected correlation functions,

$$C(l, \tau) \equiv |D_{l+j, j}(t+\tau, t)|^2 = \langle n_{l+j, t+\tau} \rangle \langle n_{j, t} \rangle - \langle n_{l+j, t+\tau} n_{j, t} \rangle,$$

which is the Fock (exchange) contribution to the density-density correlation in a Gaussian state. $C(l, \tau)$ is a second moment of the correlation matrix D , and thus its trajectory average does not correspond to an infinite temperature state.

The equal-time correlation functions $\bar{C}(l, 0)$ in Fig. 2(d) quantitatively reflect the phase diagram in Fig. 1(b). In the conformally invariant regime, an algebraic decay of the correlation function with the square of the distance $\sim [\sin(\pi l/L)]^{-2}$ is observed. The collapse of the correlation functions for variable system sizes in the inset of Fig. 2(d) demonstrates that this $\sim [\sin(\pi l/L)]^{-2}$ scaling is observed in the thermodynamic limit $L \rightarrow \infty$. On distances $l < L_c(\gamma)$ (for volume law) or in the area-law regime, the correlations deviate significantly from the $\sim l^{-2}$ behavior, showing longer-ranged or short-ranged correlations, respectively.

BKT transition and critical point.—In unitary quantum dynamics, the scenario of a phase transition from an

extended conformally invariant phase to an area-law phase via the generation of a scale in (1 + 1) dimensions is an unambiguous and exclusive feature of the BKT mechanism [52]. The measurement-induced phase transition reported here displays several similarities to this phenomenology, including the sudden drop of the effective central charge [and of the mutual information, Fig. 2(a) inset] and the loss of conformality, accompanied by the emergence of a length scale ξ in the correlation functions $C(l, 0) \sim \exp(-l/\xi)$ [Figs. 2(b) and 2(c)].

Inspired by this similarity, we perform a finite size scaling analysis of the entanglement entropy and the effective central charge $c(\gamma)$, for which we assume a BKT-type correlation length $\xi \sim \exp(-\alpha/\sqrt{|\gamma - \gamma_c|})$. Here $|\gamma - \gamma_c|$ is the distance from the measurement-induced critical point. For the entanglement entropy, this yields the scaling form $S_{\text{vN}}(\gamma, L/2) - S_{\text{vN}}(\gamma_c, L/2) = F[(\gamma - \gamma_c) \log(L)^2]$ [53,54] with a scaling function F . We observe a convincing collapse for a range of critical rates γ_c , with the best fit $\gamma_c = 0.31$ being displayed in Fig. 3(b).

The central charge is expected to be zero for $\gamma > \gamma_c$ and to display a sudden jump at $\gamma = \gamma_c$ in the limit $L \rightarrow \infty$, analogous to the quantum phase transition in equilibrium. Observables undergoing such a sudden jump at the critical point are well described by a scaling function $\tilde{F}(X)$ with argument $X = \log(L) - \alpha/\sqrt{\gamma - \gamma_c}$ [55]. The scaling collapse is shown in Fig. 3(c) for the product $\gamma c(\gamma)$. It covers two limits: (i) the case $\gamma > \gamma_c$ and $L \rightarrow \infty$ corresponds to $X \rightarrow \infty$ and therefore $c(\gamma) = 0$, (ii) the case $L < \infty$ and $\gamma \rightarrow \gamma_c$ corresponds to $X \rightarrow -\infty$ and roughly $\lim_{X \rightarrow -\infty} \gamma c(\gamma) \rightarrow 2$, according to Fig. 3(c). Overall it predicts a jump of the effective central charge at $\gamma = \gamma_c$ and a critical value $c(\gamma_c) = 2/\gamma_c$.

The finite size collapse and the scaling behavior of the central charge work well for a range of critical couplings $\gamma_c \in [0.20, 0.35]$ with the best results obtained for $\gamma_c = 0.31$. Without additional analytical constraints (such as, e.g., an analog of the Nelson-Kosterlitz criterion [56]), the precise location of the critical point is, however, still hard to determine more accurately. This is a general problem of phase transitions with slowly diverging length scales. Nevertheless, Fig. 3 provides strong indications for a phase transition of the BKT universality class. The observation of an entanglement transition from a logarithmic to area-law regime modifies the conclusion of earlier work on free fermions, which ruled out a volume-law phase under monitoring and concluded an area law for any $\gamma > 0$ [27].

Importance of true measurements.—We compare three different evolution protocols, two of which correspond to a physical measurement dynamics (QSD and QJ) and one to a nonunitary circuit evolution (QSDc) without measurement backaction. All three yield qualitatively similar results in the conformally invariant regime, $\gamma \leq \gamma_c$ [see Fig. 1(d) for QSDc and Ref. [41] for QJ]. However, only the physical

measurement protocols exhibit a transition toward an area-law phase at larger monitoring rates $\gamma \geq \gamma_c$. The QSDc indicates no area-law transition; instead the conformal invariance is extended to arbitrary $\gamma > 0$. This behavior is rooted in the absence of measurement dark states in the QSDc evolution.

In the absence of the Hamiltonian, both QSD and QJ display a set of measurement dark states $\{|\psi_D\rangle\}$, i.e., eigenstates of all measurement operators $n_l|\psi_D\rangle = \lambda_l|\psi_D\rangle$. For instance, in the QSD evolution $\hat{M}_{l,i}|\psi_D\rangle = 0$, and therefore $|\psi_D\rangle$ is an attractor of the dynamics in the strong monitoring limit $\gamma \gg J$. This reflects the tendency of a repeatedly measured system to eventually collapse into eigenstates of the measured operators. For continuous measurements, this collapse requires a measurement back-action, which is absent in the QSDc evolution. In this case, higher moments of the correlation matrix D will show a significant deviation from a physical measurement dynamics, for instance, in the norm of the state and the entanglement entropy [41]. A significant difference arises also in the distribution function of higher moments. The distribution function for the trajectory entanglement entropy, for instance, undergoes a qualitative change at the phase transition in the QSD evolution, while it remains unmodified for the QSDc evolution [41].

Discussion and conclusion.—A natural model of continuously monitored, free fermions can realize an entanglement phase transition with strong indications of BKT universality. Instead of interpolating between volume- and area-law behavior, the transition connects a “gapless” phase with conformal invariance and a logarithmic scaling of the entanglement entropy to an area law. Beyond exhibiting the characteristic phenomenology of entanglement transitions, it manifests in the behavior of connected correlations functions of the continuously monitored observables. We show that this entanglement transition also appears in a free-fermion dynamics with spatiotemporal disorder [41], which demonstrates that the entanglement scenario drawn for this model is not peculiar to an integrable tight-binding Hamiltonian.

Our results open intriguing lines for future research: The simplicity of the model and the connections to CFT and the Kosterlitz-Thouless scenario of an extensive critical regime [52], cut off at a critical monitoring rate γ_c , spark the hope to understand the transition and its variants observed in unitary circuit models of free fermions [57] and in a Dirac field theory [58] more deeply, and to find a way toward experimental detectability.

We acknowledge support from the Deutsche Forschungsgemeinschaft (DFG, German Research Foundation) under Germany’s Excellence Strategy Cluster of Excellence Matter and Light for Quantum Computing (ML4Q) EXC 2004/1 390534769, and by the DFG Collaborative Research Center (CRC) 183 Project No. 277101999–project B02. S.D. and O.A.

acknowledge support by the European Research Council (ERC) under the Horizon 2020 research and innovation program, Grant Agreement No. 647434 (DOQS). M. B. acknowledges funding via Grant No. DI 1745/2-1 under DFG SPP 1929 GiRyd. The code for our numerical computations was written in JULIA [59]. We furthermore thank the Regional Computing Center of the University of Cologne (RRZK) for providing computing time on the DFG-funded High Performance Computing (HPC) system CHEOPS as well as support.

-
- [1] B. R. Mollow, *Phys. Rev. A* **12**, 1919 (1975).
 - [2] R. H. Dicke, *Am. J. Phys.* **49**, 925 (1981).
 - [3] D. Leibfried, R. Blatt, C. Monroe, and D. Wineland, *Rev. Mod. Phys.* **75**, 281 (2003).
 - [4] V. N. Golovach, A. Khaetskii, and D. Loss, *Phys. Rev. Lett.* **93**, 016601 (2004).
 - [5] D. D. Sukachev, A. Sipahigil, C. T. Nguyen, M. K. Bhaskar, R. E. Evans, F. Jelezko, and M. D. Lukin, *Phys. Rev. Lett.* **119**, 223602 (2017).
 - [6] A. Nahum, J. Ruhman, S. Vijay, and J. Haah, *Phys. Rev. X* **7**, 031016 (2017).
 - [7] B. Skinner, J. Ruhman, and A. Nahum, *Phys. Rev. X* **9**, 031009 (2019).
 - [8] Y. Li, X. Chen, and M. P. A. Fisher, *Phys. Rev. B* **98**, 205136 (2018).
 - [9] A. Chan, R. M. Nandkishore, M. Pretko, and G. Smith, *Phys. Rev. B* **99**, 224307 (2019).
 - [10] S. Choi, Y. Bao, X.-L. Qi, and E. Altman, *Phys. Rev. Lett.* **125**, 030505 (2020).
 - [11] C.-M. Jian, Y.-Z. You, R. Vasseur, and A. W. W. Ludwig, *Phys. Rev. B* **101**, 104302 (2020).
 - [12] M. J. Gullans and D. A. Huse, *Phys. Rev. X* **10**, 041020 (2020).
 - [13] A. Zabalo, M. J. Gullans, J. H. Wilson, S. Gopalakrishnan, D. A. Huse, and J. H. Pixley, *Phys. Rev. B* **101**, 060301(R) (2020).
 - [14] L. Zhang, J. A. Reyes, S. Kourtis, C. Chamon, E. R. Mucciolo, and A. E. Ruckenstein, *Phys. Rev. B* **101**, 235104 (2020).
 - [15] Q. Tang and W. Zhu, *Phys. Rev. Research* **2**, 013022 (2020).
 - [16] Y. Bao, S. Choi, and E. Altman, *Phys. Rev. B* **101**, 104301 (2020).
 - [17] Y. Li, X. Chen, and M. P. A. Fisher, *Phys. Rev. B* **100**, 134306 (2019).
 - [18] M. J. Gullans and D. A. Huse, *Phys. Rev. Lett.* **125**, 070606 (2020).
 - [19] A. Nahum and B. Skinner, *Phys. Rev. Research* **2**, 023288 (2020).
 - [20] M. Szyniszewski, A. Romito, and H. Schomerus, *Phys. Rev. B* **100**, 064204 (2019).
 - [21] S. Goto and I. Danshita, *Phys. Rev. A* **102**, 033316 (2020).
 - [22] Y. Li, X. Chen, A. W. W. Ludwig, and M. P. A. Fisher, [arXiv:2003.12721](https://arxiv.org/abs/2003.12721).
 - [23] V. Alba and F. Carollo, *Phys. Rev. B* **103**, L020302 (2021).
 - [24] Y. Fuji and Y. Ashida, *Phys. Rev. B* **102**, 054302 (2020).
 - [25] X. Chen, Y. Li, M. P. A. Fisher, and A. Lucas, *Phys. Rev. Research* **2**, 033017 (2020).

- [26] M. Szyniszewski, A. Romito, and H. Schomerus, *Phys. Rev. Lett.* **125**, 210602 (2020).
- [27] X. Cao, A. Tilloy, and A. De Luca, *SciPost Phys.* **7**, 024 (2019).
- [28] M. Knap, *Phys. Rev. B* **98**, 184416 (2018).
- [29] D. Yang, C. Laflamme, D. V. Vasilyev, M. A. Baranov, and P. Zoller, *Phys. Rev. Lett.* **120**, 133601 (2018).
- [30] D. Yang, C. Laflamme, D. V. Vasilyev, M. A. Baranov, and P. Zoller, *Phys. Rev. Lett.* **120**, 133601 (2018).
- [31] I. de Vega and D. Alonso, *Rev. Mod. Phys.* **89**, 015001 (2017).
- [32] H. M. Wiseman and G. J. Milburn, *Phys. Rev. A* **47**, 1652 (1993).
- [33] J. Dalibard, Y. Castin, and K. Mølmer, *Phys. Rev. Lett.* **68**, 580 (1992).
- [34] M. Ippoliti, M. J. Gullans, S. Gopalakrishnan, D. A. Huse, and V. Khemani, *Phys. Rev. X* **11**, 011030 (2021).
- [35] Results represent averages over 500 trajectories for $L \leq 600$ and 300 trajectories for $L = 800$.
- [36] N. Gisin and I. C. Percival, *J. Phys. A* **25**, 5677 (1992).
- [37] L. Diósi, N. Gisin, and W. T. Strunz, *Phys. Rev. A* **58**, 1699 (1998).
- [38] C. M. Caves and G. J. Milburn, *Phys. Rev. A* **36**, 5543 (1987).
- [39] The QSDc evolution is realized by setting $\hat{M}_{l,t} = n_l$.
- [40] A. J. Daley, *Adv. Phys.* **63**, 77 (2014).
- [41] See Supplemental Material at <http://link.aps.org/supplemental/10.1103/PhysRevLett.126.170602> for numerical results of the QJ evolution, an analysis of the auto-correlation functions, and a discussion of the importance of probability conservation, which includes Ref. [42].
- [42] M. V. Regemortel, Z.-P. Cian, A. Seif, H. Dehghani, and M. Hafezi, [arXiv:2008.08619](https://arxiv.org/abs/2008.08619).
- [43] P. Calabrese and J. Cardy, *J. Stat. Mech.* (2005) P04010.
- [44] V. Alba and P. Calabrese, *SciPost Phys.* **4**, 17 (2018).
- [45] P. Calabrese and J. Cardy, *J. Stat. Mech.* (2004) P06002.
- [46] P. Calabrese and J. Cardy, *J. Phys. A* **42**, 504005 (2009).
- [47] J. Cardy and J. L. Jacobsen, *Phys. Rev. Lett.* **79**, 4063 (1997).
- [48] G. Refael and J. E. Moore, *Phys. Rev. Lett.* **93**, 260602 (2004).
- [49] N. Laflorencie, *Phys. Rev. B* **72**, 140408(R) (2005).
- [50] J. Cardy, *Phys. Rev. Lett.* **84**, 3507 (2000).
- [51] M. M. Wolf, F. Verstraete, M. B. Hastings, and J. I. Cirac, *Phys. Rev. Lett.* **100**, 070502 (2008).
- [52] D. B. Kaplan, J.-W. Lee, D. T. Son, and M. A. Stephanov, *Phys. Rev. D* **80**, 125005 (2009).
- [53] K. Harada and N. Kawashima, *Phys. Rev. B* **55**, R11949 (1997).
- [54] J. Carrasquilla and M. Rigol, *Phys. Rev. A* **86**, 043629 (2012).
- [55] A. W. Sandvik, A. Avella, and F. Mancini, *AIP Conf. Proc.* **1297**, 135 (2010).
- [56] Y.-D. Hsieh, Y.-J. Kao, and A. W. Sandvik, *J. Stat. Mech.* (2013) P09001.
- [57] Y. Bao, S. Choi, and E. Altman, [arXiv:2102.09164](https://arxiv.org/abs/2102.09164).
- [58] M. Buchhold, Y. Minoguchi, A. Altland, and S. Diehl, [arXiv:2102.08381](https://arxiv.org/abs/2102.08381).
- [59] J. Bezanson, A. Edelman, S. Karpinski, and V. B. Shah, *SIAM Rev.* **59**, 65 (2017).